

Lawrence Berkeley National Laboratory

LBL Publications

Title

Iodine solubility in a low-activity waste borosilicate glass at 1000°C

Permalink

<https://escholarship.org/uc/item/4qj535x9>

Journal

Journal of Nuclear Materials, 452(1-3)

ISSN

00223115

Authors

Riley, Brian J.
Schweiger, Michael J.
Kim, Dong-Sang
[et al.](#)

Publication Date

2014-09-01

Iodine solubility in low-activity waste borosilicate glass

Brian J. Riley,^{*,†} Michael J. Schweiger,[†] Dong-Sang Kim,[†]

Wayne W. Lukens, Jr.,[‡] Benjamin D. Williams,[†] Cristian Iovin,[†] Carmen P. Rodriguez,[†]

Nicole R. Overman,[†] Mark E. Bowden,[†] Derek R. Dixon,[†] Jarrod V. Crum,[†] John S. McCloy,[§]

and Albert A. Kruger^{**}

[†]*Pacific Northwest National Laboratory, Richland, WA 99352*

[‡]*Lawrence Berkeley National Laboratory, Berkeley, CA 94720*

[§]*Washington State University, Pullman, WA 99164*

^{**}*DOE-WTP Project Office Engineering Division, Richland, Washington 99352*

Keywords: iodine, solubility, low-activity waste, borosilicate glass

Abstract

The purpose of this study was to determine the solubility of iodine in a low-activity waste borosilicate glass when heated inside an evacuated and sealed fused quartz ampoule. The iodine was added to glass frit as KI in quantities of 100–24000 ppm iodine (by mass), each mixture was added to an ampoule, the ampoules were heated at 1000 °C for 2h, and then air quenched. In samples with ≥ 12000 ppm iodine, low viscosity salt phases were observed on the surface of the melts during cooling that solidified into a white coating upon cooling. These salts were identified as mixtures of KI, NaI, and Na₂SO₄ with X-ray diffraction (XRD). The iodine concentrations in glass specimens were analyzed with inductively-coupled plasma mass spectrometry and the overall iodine solubility was determined to be 10000 ppm by mass. Several crystalline inclusions

*Corresponding author: Brian J. Riley; brian.riley@pnl.gov; +1 (509)372-4651 (phone), +1 (509)372-5997 (fax)

of iodine sodalite, $\text{Na}_8(\text{AlSiO}_4)_6\text{I}_2$, were observed in the 24000 ppm specimen as determined by micro-XRD and wavelength dispersive spectroscopy.

1 INTRODUCTION

The Hanford Site in Washington State contains a large volume of residual waste from nuclear weapons production. The current pathway to immobilize the low-activity radioactive waste (LAW) fraction is vitrification. This waste stream is composed of several constituents that cause complications during the vitrification process due to the formation of a separate low viscosity salt phase, known as *yellow phase*. This salt phase is primarily composed of alkali metal salts of halides and oxyanions (e.g., CrO_4^{2-} , ReO_4^- , SO_4^{2-} , TcO_4^-) [1-13]. Technetium-99 (^{99}Tc) and iodine-129 (^{129}I) are of particular concern because their high volatility can result in low retention in glass during the LAW vitrification process. The major environmental concern with ^{99}Tc and ^{129}I is their rapid dispersion in air or water under the right conditions and their long half-lives ($t_{1/2}$), $t_{1/2} = 2.1 \times 10^5$ y for ^{99}Tc and $t_{1/2} = 1.6 \times 10^7$ y for ^{129}I . Performance assessments conducted to provide guidance to the storage and disposal project for Hanford LAW show that ^{129}I is the primary dose contributor during the first 5,000 years following disposal [14].

The fraction remaining in the melt relative to the original concentration is defined as the *retention ratio*, R_i , which is determined with Equation (1) where $g_{i,r}$ is the mass fraction measured after melting and $g_{i,0}$ is the target mass fraction of the i -th species [15].

$$R_i = g_{i,r}/g_{i,0} \quad (1)$$

Retention of halides in sodium aluminum borosilicate glasses decreases consistently with increasing ionic radius where iodine has the lowest retention of the halides, i.e., $\text{F} > \text{Cl} > \text{Br} > \text{I}$ [15, 16]. Recent scaled melter tests with various simulated LAW glass feeds spiked with 1000 ppm iodine by mass showed that the retention ratio of iodine in LAW glass is approximately

20%, on average [17].

The retention of a particular component within a glass melt can be limited by a number of factors, (1) a slow incorporation rate into the glass melt during the melting process possibly due to its low solubility (kinetic effects), (2) preferential partitioning into a separated salt phase (thermodynamic solubility), and (3) high volatilization due to its high vapor pressure or weak bonding to the glass network (volatility). Halide solubility was observed to decrease with increasing ionic radius among the halides ($F > Cl > I$) as presented by Crichton et al. [18] when studying a similar glass composition as that in the current work. They reported that the loss of iodine due to volatilization was a major problem even at 900 °C. Dark bubbles, presumably filled with $I_2(g)$, were observed in glasses containing > 2000 ppm iodine (by mass). By this criterion, they determined the solubility of iodine to be ~ 2000 ppm (by mass). However, iodine concentrations of 5000–8200 ppm were observed with electron probe microanalysis (EPMA) in the glasses with target compositions of 10000 ppm iodine. This inconsistency and the problem of high volatilization under the open crucible melting (although with a lid) used in the aforementioned study raise a potential issue for the reported iodine solubility. Specifically, whether the iodine solubility in these studies was determined by volatility or by thermodynamic solubility. Riley et al. [19] provided additional discussion on the correlations between the halides and their respective retentions, solubilities, ionic radii, and bond dissociation energies based on data in the literature [16, 18, 20].

The solubilities of Re [6, 7] and ^{99}Tc [13, 21] in LAW glass were recently determined by melting glass frit with added $KReO_4$ or $KTcO_4$ in evacuated, sealed fused quartz ampoules. Sealed ampoules were used to avoid volatile losses during heat treatment at high temperatures. The solubilities were found to be 3000 ppm for Re [6] and 2000–2800 ppm for ^{99}Tc [13] by mass

(~20 mmol/kg in both cases). In the current work, the same approach was used to determine the solubility of iodine in LAW glass. By limiting volatilization, these solubility studies show the extent to which the retention ratios of these volatile constituents are controlled by their thermodynamic solubility in glass.

2 EXPERIMENTAL METHODS

2.1 *Glass fabrication*

The starting material for these experiments was a LAW borosilicate glass that was synthesized with a melt-quench technique. The *baseline* glass, or the glass without any iodine additions, was made in a large batch from the appropriate amounts of oxides (Al_2O_3 , Cr_2O_3 , Fe_2O_3 , MgO , SiO_2 , TiO_2 , ZnO , ZrO_2), carbonates (CaCO_3 , K_2CO_3 , Na_2CO_3), H_3BO_3 , and Na_2SO_4 (Table 1). The glass batch was homogenized in a vibrating agate mill and melted in a Pt/10%Rh crucible at 1200 °C for 1 h in a Deltech furnace (Deltech, Inc., Denver, CO). The resulting glass was quenched on an Inconel plate and crushed using a tungsten carbide mill within a vibratory mixer yielding a fine, homogeneous glass powder (<40 μm).

Iodine was added as KI (ChemWest, ~0.5 mm, ACS reagent grade). The target concentration of iodine added to the baseline glass was varied between 100 and 24000 ppm (see Table 1), defined as parts per million of iodine atoms in the glass (by mass). Except for the 100 and 1000 ppm samples, KI was hand-ground in an agate mortar and pestle to a fine powder prior to mixing it with the glass frit. The initial tests with 100 and 1000 ppm iodine used granular KI, which resulted in a few KI particles that did not fully react with glass during the 2 h heat treatment. The relative ratios of the other components in the glasses with added iodine remained unchanged, and their concentrations were renormalized after accounting for the added KI. The LAW glass powder and the specified amount of KI were mixed in an agate mill for a total mass

of 20 g for each experiment. The glass frit was prepared this way so that the iodine was well-mixed within the glass and captured by the glass powder minimizing kinetic effects in controlling the iodine solubility.

Each batch of glass powder was placed into a flat-bottomed, fused quartz tube, and a fused quartz end cap was inserted into the tube as shown in Figure 1. The tube was then connected to a vacuum system and evacuated. Once the pressure was $\sim 10^{-4}$ Pa, the tube was sealed with an oxygen-propane torch. This vacuum-sealed tube will hereafter be referred to as the *ampoule*. After sealing, three type-K thermocouples (OMEGA, Stamford, CN) were connected to the outside of the ampoule with stainless steel wire for temperature monitoring at top, middle and bottom of melt during the heat treatment. The ampoule was then inserted in a Deltech furnace pre-heated to 750 °C. The temperature of the furnace was increased from 750 °C to 1000 °C at a heating rate of 5 °C min⁻¹, followed by a dwell of 2 h at 1000 °C. After the dwell, the furnace temperature was lowered to 900 °C for a few minutes, and the ampoule was removed from the furnace and quenched in air within a stainless steel canister. In a separate experiment, a 24000 ppm iodine glass was processed the same as previously described with one difference; instead of air quenching the ampoule, it was plunged into a stainless steel canister full of deionized water.

2.2 Preparation for analysis

Once the ampoule was cooled to room temperature, small pieces were removed and set aside for analysis. The remainder of the sample was vacuum-impregnated with EpoThin resin (Buehler, Lake Bluff, IL). Once hardened, a ~ 5 –7 mm thick section was removed from the center of the cylindrical ingot with a diamond wire saw (CT400, Diamond Wire Technology, LLC, Colorado Springs, CO). The section was polished with an LP-01 Syntron vibratory polisher

(FMC Technologies, Saltillo, MS) to a 1 μm finish in glycol-based diamond suspensions.

2.3 *Chemical analysis*

From each experiment, specimens without visually identifiable inclusions were powdered and analyzed for iodine concentration by inductively-coupled plasma mass spectrometry (ICP-MS) using a Perkin Elmer Elan DRC II (Elemental Scientific, Omaha, NE). Specimens with visually identifiable inclusions were found and analyzed by ICP-MS for comparison to samples without inclusions.

Specimens were prepared and analyzed using a technique developed at PNNL for quantifying iodine [22]. Specimens were ground to a powder in a tungsten carbide mill, and 0.01 g of ground glass sample was added to each of two nickel crucibles followed by 5 mL of flux solution containing 40% KOH and 4% KNO₃. Moisture was removed from the flux solution by placing the crucibles in a 150 °C drying oven for 2 hours. Crucibles were transferred to a 200 °C furnace that was heated to 550 °C over 45 min. Then, the crucibles were held at 550 °C for 1 h and cooled.

Crucibles were rinsed into 50 mL centrifuge tubes with 5–10 mL of deionized water. The crucible was then rinsed with 5 mL of 1:1 concentrated H₂SO₄ and 1 M NaHSO₃ (added as Na₂S₂O₅) solution, which was added to the centrifuge tube. The crucible was rinsed into the centrifuge tube one last time with deionized water. The contents of the tube were brought to a final volume of 30–35 mL. The contents of the centrifuge tubes were analyzed for ¹²⁷I with ICP-MS.

2.4 *X-ray absorption near-edge spectroscopy*

X-ray absorption near-edge spectroscopy (XANES) was performed on chunks of selected

glasses and powdered iodine standards to identify iodine species. Data were obtained at the Stanford Synchrotron Radiation Lightsource (SSRL) BL 11-2 in transmission (standards) and fluorescence (glass). Data were obtained from 300 eV below the iodine K-edge to 1000 eV above the edge; the data from 75 eV below the edge to 200 eV above the edge was obtained with 0.35 eV spacing. The rest of the data points were widely spaced (50 eV) and were used for the pre- and post-edge corrections.

The monochromator was detuned 50% to reduce the harmonic content of the beam. Transmission data was obtained using Ar-filled ion chambers. Fluorescence data was obtained using a 100-element Ge detector and were corrected for detector dead time and self-absorption. Data were reduced from raw data to spectra using SixPack, [23] and spectra were normalized using Artemis [24]. Normalized spectra were fit using standard spectra in the locally written program 'Fites'. Standard spectra were energy-calibrated using NaIO₃ as the energy reference. Sample spectra were allowed to vary in energy during fitting. The spectral resolution was 10 eV based on the width of the NaIO₃ pre-edge peak.

The iodide and iodate standards were prepared by finely grinding the compound with boron nitride then placing the mixture in an aluminum holder sealed with Kapton tape. All samples were dried under vacuum and were prepared in an inert atmosphere glovebox and stored in a sealed glass jar until just prior to data collection. The iodine sample was prepared by mixing iodine crystals and boron nitride in a glass vial, heating the vial to 120 °C for 5 minutes then allowing the vial to cool to room temperature. The mixture was heat sealed inside a thick walled polyethylene tube (disposable pipette). Glass samples were mounted directly to a sample holder using a tape adhesive.

2.5 X-ray diffraction

X-ray diffraction (XRD) was conducted on selected glass and salt samples with a Bruker® D8 Advance (Bruker AXS Inc., Madison, WI) XRD with Cu K α emission ($\lambda = 1.5406$ Å). The detector used was a LynxEye™ position-sensitive detector with a collection window of $3^\circ 2\theta$. The scan parameters for the glass powders (100–24000 ppm iodine) were 5 – $90^\circ 2\theta$ with a step of $0.015^\circ 2\theta$ and a 1.0-s dwell at each step using a 12 mm variable divergent slit. Salts were analyzed in powder mounts at 5 – $70^\circ 2\theta$ with a step of $0.015^\circ 2\theta$ and a 0.3-s dwell at each step. The salt from the 8000 ppm iodine specimen was analyzed in a sealed 0.6-mm capillary tube at 10 – $80^\circ 2\theta$ with a step of $0.015^\circ 2\theta$ and a 3-s dwell at each step. Bruker AXS DIFFRAC^{plus} EVA and Topas software programs were used to identify and quantify the crystalline phases, respectively.

Additionally, micro-XRD analysis was conducted on the air-quenched 24000 ppm iodine glass sample with a Rigaku D/Max Rapid II micro diffraction system (Rigaku Americas Corporation, The Woodlands, TX). X-rays were generated (MicroMax 007HF operated at 35 kV and 25 mA) from a rotating Cr target ($\lambda = 2.2910$ Å) and focused through a 300 μm diameter collimator into the specimen. The incident beam direction was fixed at 25° to the sample surface and the diffracted intensities were recorded on a large 2D image plate. The 2D images were integrated between 25 – $150^\circ 2\theta$ to give powder patterns.

2.6 Scanning electron microscopy

A JEOL JSM-7001F field-emission gun microscope (JEOL USA, Inc. Peabody, MA) was used to perform scanning electron microscopy (SEM) analysis on select samples. Additionally, an EDAX Si-drift detector was used to conduct energy dispersive spectroscopy (EDS; Apollo XL, AMETEK, Berwyn, PA) for elemental spot analysis and dot mapping.

2.7 Electron probe microanalysis and wavelength dispersive spectroscopy

A JEOL JXA-8530F HyperProbe EPMA with a field emission gun and five wavelength dispersive spectrometers (WDSs) was used to conduct area and spot analysis on a polished cross-section of the air-quenched 24000 ppm iodine glass sample. The electron beam was set at an accelerating voltage of 15 keV and a current of 15 nA. Quantification utilized a ZAF data reduction routine (EPMA Analysis, JEOL) that corrected and quantified characteristic X-ray yields against mineral standards (Geller Microanalytical Laboratory, Inc., Topsfield, MA). The specific standards were: SiO₂ for Si, corundum (Al₂O₃) for Al, orthoclase (KAlSi₃O₈) for K, NaCl for Na, and the 24000 ppm iodide glass specimen for I to identify specific peak locations.

3 RESULTS AND DISCUSSION

3.1 General observations

After each ampoule was removed from the furnace, the glass inside went from glowing red to an opaque black as it cooled. In all glasses except the water-quenched 24000 ppm iodine glass, a dimple formed at the top of the melt upon cooling, which is typical for glass that is air-cooled in a canister. For glasses with as little as 1000 ppm iodine, a faint purple gas was observed inside the ampoule when it was removed from the furnace, which faded as the ampoule cooled. This purple haze was observed in all experiments with an increasingly dark purple color at higher iodine concentrations, providing evidence of unincorporated I₂(g). As the ampoule cracked and air penetrated the plenum space, the ampoule walls above the glass turned yellow-brown (1000 to 4000 ppm I) to brown (\geq 8000 ppm I glasses). The brown color dissipated after the ampoule was exposed to air for ~24 h.

For glasses with \geq 12000 ppm iodine, a low viscosity, clear liquid was observed at the top

of the melt, which pooled into the dimple and solidified into a white layer on top of the glass upon cooling. This layer appears very similar to that observed in the Re [6, 7] and ^{99}Tc [13] solubility experiments when the amount of added Re or ^{99}Tc exceeded their solubilities in the glass.. The quantity and thickness of this layer increased with iodine loading from 12000 \rightarrow 16000 \rightarrow 24000 ppm, which suggests that the glass melts with ≥ 12000 ppm iodine were saturated with iodine at 1000 °C.

3.2 Bulk glass analysis

3.2.1 Morphology

In some cases, a full cross-sectional image of the samples could not be obtained due to the severe fracturing that occurred when each sample was cooled. A collage of the 100, 1000, 12000, and 24000 ppm water-quenched samples is presented in Figure 2. While cross-sections of the 16000 and 24000 ppm air-quenched samples are not shown, these samples appeared very similar to the 12000 ppm sample. These images reveal that the samples with increasing iodine concentrations had higher fractions of bubbles throughout the bulk as shown by the progression of bubble volume in samples with increasing iodine loadings (Figure 2). The 24000 ppm water-quenched sample had a very high fraction of bubbles throughout the bulk and lacked the characteristic dimple at the top. In this case, the exterior of the glass specimen solidified first and the decrease in volume of the cooling glass resulted in hundreds of small bubbles throughout the sample making it difficult to visualize any potential inclusions.

3.2.2 XRD analysis

As seen in Figure 3, the bulk XRD analysis of glass samples did not show any diffraction peaks. The diffraction patterns had broad peaks centered around $30\text{--}31^\circ 2\theta$ along with other

minor peaks at lower and higher angles commonly observed with borosilicate glasses. The diffraction patterns were very similar at different iodine loadings with slight shape variations in location and intensity to the amorphous humps.

3.2.3 XANES analysis

The XANES spectra for NaIO₃, I₂, NaI, KI, RbI, CsI, and AgI are shown in Figure 4, and molecular orbital diagrams for iodide (I⁻), iodine (I₂), and iodate (IO₃⁻) are shown in Figure 5. The spectra of NaIO₃, I₂, and KI are identical to those previously reported [25-27]. The absorption edge of the NaIO₃ is lowest in energy, followed by I₂ at slightly higher energy. The absorption edges of the iodide salts are almost identical and lie still higher in energy. The relationship between the energies of the absorption edges and the formal oxidation state of iodine is reversed from the usual order (complexes with higher formal oxidation states typically have absorption edges at higher energy). This reversal is due to the presence of a large pre-edge peak due to an allowed 1s to 5p transition. This peak is largest for NaIO₃, since the 5p orbitals of iodine are largely vacant in this formally pentavalent complex. The peak is much smaller in I₂ since the 5p orbitals contain five electrons leaving only a single hole in the σ -antibonding orbital for the 1s electron of each iodine atom. The positions of the pre-edge peaks are indicated by arrows in Figure 4. On the other hand, the 5p shell is filled in the iodide salts, so no pre-edge peak occurs below the absorption edge.

In addition to the pre-edge peak in NaIO₃ and I₂, other structure is present in all of the XANES spectra due to scattering of the outgoing photoelectron from the surrounding atoms (extended X-ray absorption fine structure, EXAFS). The EXAFS features are very strong in the case of NaIO₃, which possesses three short terminal oxide ligands. On the other hand, the EXAFS spectra are quite weak in I₂ and the alkali iodides due to the much longer distance from I

to the surrounding atoms. The frequency of the EXAFS oscillations is inversely proportional to the bond length, so only one oscillation is visible for NaIO₃ with the short I=O bonds, while between three and four oscillations are present in the spectrum of CsI.

The spectra of the iodine containing glasses are almost identical. The only real difference is that the 12000 ppm I sample has a small peak at the edge. Performing the background subtraction was problematic for this sample (the post edge region was strongly curved), and this difference may not be meaningful. The spectra of all glasses and their fits are shown in Figure 6. In all cases a good, although not perfect, fit was obtained. The glass spectra were initially fit using all seven reference spectra, but only the spectrum of NaI contributed significantly to the fit. Using all of the reference spectra simultaneously results in large standard deviations for the contribution of the reference spectra, so the fits were performed using only NaI, I₂, and NaIO₃. The results are given in Table 2. The significance of the standard spectra in the fitting the glass spectra is given by the p value of that component (the p value is the probability that the improvement to the fit is due to random error). A p-value less than 0.05 means that the contribution of that component is greater than twice the standard deviation of the fit, which is the usual criteria for significance in XANES fitting. The NaI contributed significantly ($p < 0.001$) in all cases and the contribution from I₂ is significant only when the iodine loading was ≤ 2000 ppm iodine. The detection limit is approximately twice the standard deviation or $\sim 10\%$ of the iodine species. In other words, these XANES cannot reliably determine the concentration of the species if it comprises less than 10% of the total iodine species. The 2000 ppm glass was run on all three occasions where XANES analysis was performed to assess the reproducibility of the data. As is shown in Table 2, the values for each separate analysis on this glass varied somewhat with 0.79–0.99 for NaI, 0–0.10 for I₂, and 0.01–0.11 for NaIO₃.

The XANES spectra for iodine in the glass and that from NaI standard did not agree perfectly, which is partially responsible for the relatively large uncertainties in the XANES speciation. Specifically, the EXAFS oscillations of the glass spectra are weaker and lower in frequency relative to NaI. These results suggest that the species present in the glass is iodide surrounded by sodium ions; however, the sodium ions are slightly closer to iodide than they are in the crystal structure of NaI and there are fewer sodium ions present and/or there is a larger variation in the distances between iodide and the neighboring sodium ions. The fact that the sodium iodide distance is shorter in the glasses is consistent with the hypothesis that there are fewer sodium ions surrounding the iodide in the glass than the six Na neighbors in the NaI crystal structure. The fact that the XANES spectra of the glass are not perfectly fit by the spectrum of NaI more consistent with the presence of $(\text{Na}^+)_x(\text{I}^-)$ clusters in the glass than with crystalline NaI inclusions in the glass. The presence of $(\text{Na}^+)_x(\text{I}^-)$ clusters rather than crystalline NaI inclusions is also strongly supported by the XRD analyses discussed above.

3.3 Iodide precipitates

3.3.1 Melt surface salts

A portion of the white salt mixture drained into the cracks of the glass during cooling. The mixed salt formation in the present samples saturated with iodine is analogous to the formation of Re and ^{99}Tc salts observed during their respective solubility experiments [6, 7, 13]. Similarly, a separate sulfate salt phase is formed during melter processing of waste glass feeds when the amount of sulfate exceeds its solubility in the glass [1, 3].

The salt was scraped off and analyzed with XRD and XANES. The XRD of the salts from the 12000, 16000, and 24000 ppm iodine experiments analyzed in air showed mixtures of $\text{NaI}\cdot 2\text{H}_2\text{O}$, Na_2SO_4 , and KI. A typical XRD pattern for one of these salt mixtures is presented in

Figure 8 for 16000 ppm iodine. A specimen of the 24000 ppm iodine salt was analyzed in a sealed capillary tube (not shown) to confirm that the NaI was not initially hydrated. Thus, the NaI became hydrated forming NaI·2H₂O upon exposure to the atmosphere during the analysis of the specimens. The XANES analysis confirmed that the primary iodine configuration was in the presence of Na instead of K (NaI, Table 2). This suggests that KI, the source of added iodine, underwent ion-exchange with Na to form NaI, which is similar to what was observed in the KReO₄-glass system [6, 28].

3.3.2 Iodine inclusions

Figure 9 shows an example of the inclusions found within the glasses with ≥ 8000 ppm iodine. In samples containing 8000 and 12000 ppm iodine, the inclusions were few, large, and ellipsoidal ranging in size at 100–250 μm along the longest axis. At higher concentration of 16000 and 24000 ppm iodine, very small inclusions were observed in addition to the large inclusions. The very small inclusions were too small to analyze individually but the larger inclusions were visible on the polished surface or were only slightly below the surface and could be extracted with tweezers for further analysis. An SEM micrograph and a WDS area map were collected of a cross-sectioned inclusion, and the results are presented in Figure 10. This inclusion was also analyzed with micro-XRD and determined to be a NaI-based sodalite with a composition of Na₈(AlSiO₄)₆I₂, space group $P\bar{4}3n$, and unit cell $a = 0.9027$ nm by Rietveld refinement (Figure 11) [29]. The structure of NaI-based sodalite consists of Na-Al-Si-O cages with iodine atoms in the center and corners of the unit cell shown in Figure 12.

The composition of this inclusion, as determined by spot WDS analysis on inclusions from the 24000 ppm iodine specimen (Figure 10) is in good agreement with the nominal composition Na₈(AlSiO₄)₆I₂ as shown in Figure 13. Other, similarly extracted inclusions were

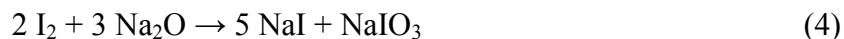
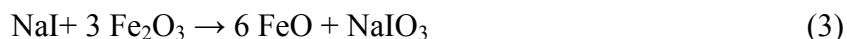
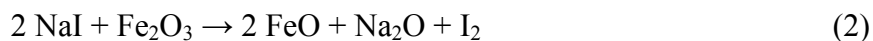
determined to be $\text{Na}_8(\text{AlSiO}_4)_6\text{I}_2$ with EDS (not shown). In all cases, these inclusions resembled bubbles by optical microscopy, but when cross-sectioned the inclusions were not hollow. Instead, the inclusions consist of clusters of smaller sodalite crystals $\sim 1\text{--}10\ \mu\text{m}$ in size surrounding a pocket of glass with a slightly different composition than the bulk glass (Figure 10). The WDS map in Figure 10 shows that the sodalite crystals did not contain K and the Al concentration was higher within the sodalite.

It was not clear whether these sodalite inclusions formed upon soaking at $1000\ \text{°C}$ or upon cooling. Thus, a 24000 ppm iodine sample was prepared but was water quenched instead of being air quenched. Unfortunately, the extremely high number of bubbles present in the water-quenched specimen made the search for inclusions impossible. Because the sodalite is likely to dissolve in the glass melt at $1000\ \text{°C}$, the sodalite most likely formed during cooling, but additional testing was not performed to support this hypothesis.

3.4 Iodine speciation

Various forms of iodine were observed with XANES and XRD. The XANES analysis of the glass specimens showed that the contribution from iodide was significant below 2000 ppm, but iodate was only significant for a single specimen. The presence of I_2 in contact with the melt is consistent with the characteristic purple gas, which was observed inside the ampoule upon removal from the furnace. In order for I_2 or IO_3^- to be present in glass, the starting material would require oxidation from I^- to I^0 or I^{5+} , respectively. One potential oxidant is Fe^{3+} , which comprises $\sim 5\%$ of the glass by mass, as shown in Equations (2) and (3). In previous experiments using the same glass frit, 95.5% of the iron was initially present at Fe^{3+} , which decreased to 87% after that frit was run in the baseline experiment at $1000\ \text{°C}$ under vacuum in a sealed quartz ampoule. The initial frit and the frit subjected to melting under vacuum both contain a large

excess of Fe^{3+} relative to Fe^{2+} , which could be responsible for the oxidation of iodide observed in this study. Another potential redox reaction is the disproportionation of I_2 to NaI and NaIO_3 as shown in Equation (4).



3.5 Solubility

The full data set of measured versus targeted iodine concentration as quantified by ICP-MS is presented in Figure 12, where the iodine solubility was determined to be ~10000 ppm, by mass. As shown by XANES, the vast majority of iodine in the glass is present as iodide, and the solubility measurement is primarily for this species. Several other conclusions can be drawn from Figure 12. First, the measured versus targeted iodine follows a linear (measured:target = 1:1) trend from 100–2000 ppm iodine but then deviates slightly up to 12000 ppm due to the loss of iodine in the head space of the sample above the melt. Secondly, the measurements performed on specimens with inclusions show higher, but not increasingly higher, values with increased iodine loadings. Finally, when the amount of added iodide exceeded the thermodynamic solubility, a separate mixed salt phase formed at the top of the melt.

4 CONCLUSIONS

The solubility of iodine in a low-activity waste borosilicate glass was determined in evacuated and sealed fused quartz ampoules heat treated at 1000 °C for 2 h. Under these conditions, loss of elemental iodine was minimized, and iodine was primarily present as iodide. Iodide loadings ranged 100–24000 ppm, by mass. The solubility of iodide measured in the present study (10000 ppm iodide, by mass) is almost an order of magnitude higher than

previously reported for a comparable glass (~2000 ppm iodine). Since the estimated iodine concentration in Hanford low-activity waste glass is roughly 0.3 ppm, on average, if 100% retained (based on the projected total mass of ^{129}I , 180 kg {Mann, 2004 #28}, and the estimated total mass of low-activity waste glass to be produced, 5.3×10^8 kg {Certa, 2011 #32}), it can be concluded that the retention of iodide in a low-activity waste glass is not limited by solubility. However, the present results cannot conclude that iodine will be effectively retained during production of low-activity waste glass. As noted in the introduction, three factors control the retention of radionuclides in the glass: kinetic factors, thermodynamic solubility, and volatilization. In this study, kinetic factors and volatilization have been minimized to determine the thermodynamic solubility. In order to predict the retention of iodine during glass production, kinetic factors and volatilization need to be examined. In the present study, some volatility was observed due to the formation of elemental iodine, presumably due to oxidation by Fe^{3+} in the glass frit. During production of low-activity waste glass, conditions in the glass are expected to be highly oxidizing due to the decomposition of nitrate. These conditions may decrease the retention of iodine in the waste glass due to oxidation of iodide to elemental iodine, which is volatile under these conditions, as observed in this study.

5 ACKNOWLEDGEMENTS

This work was supported by the Department of Energy's Waste Treatment & Immobilization Plant Federal Project Office. The authors thank Clyde Chamberlin and Shelley Carlson for helping prepare the samples, David Pierce, Jesse Lang, and Steven Luksic for optical microscopy, and Jarrod Crum for help with XRD. Pacific Northwest National Laboratory is operated by Battelle Memorial Institute for the U.S. Department of Energy under contract DE-AC05-76RL01830. A portion of the research was performed using EMSL, a national scientific user facility sponsored by the Department of Energy's Office of Biological and Environmental Research and located at Pacific Northwest National Laboratory. Portions of this work were performed at Lawrence Berkeley National Laboratory under Contract No. DE-AC02-05CH11231. Portions of this research were carried out at the Stanford Synchrotron Radiation Lightsource, a

Directorate of SLAC National Accelerator Laboratory and an Office of Science User Facility operated for the U.S. DOE Office of Science by Stanford University.

6 REFERENCES

- [1] R. Goles, J. Perez, B. MacIsaac, D. Siemer, J. McCray. 2001. Test summary report INEEL sodium-bearing waste vitrification demonstration - RSM-01-1. PNNL-13522. Pacific Northwest National Laboratory, Richland, WA.
- [2] H. Li, P. Hrma, J.D. Vienna, pp. 237-245, Proc. of the Env. Issues Waste Manage. Tech. Ceram. Nucl. Ind. VI, 119. Edited by D. R. Spearing, G. L. Smith, and R. L. Putnam. St. Louis, MO, 2000.
- [3] I.L. Pegg, H. Gan, I.S. Muller, D. McKeown, K. Matlack. 2001. Summary of preliminary results on enhanced sulfate incorporation during vitrification of LAW feeds. VSL-00R3630-1. Vitreous State Laboratory, The Catholic University of America, Washington, DC.
- [4] P. Hrma, J. Vienna, J. Ricklefs, pp. 147-158, Proc. of the Mat. Res. Soc. Symp. - Sci. Basis Nucl. Waste Manage. XXVI, 757. Edited by R. J. Finch and D. B. Bullen. Boston, MA, 2002.
- [5] P. Hrma, J. Vienna, W. Buchmiller, J. Ricklefs, pp. 93-100, Proc. of the Env. Issues Waste Manage. Tech. Ceram. Nucl. Ind. IX - Ceram. Trans., 155. Edited by J. D. Vienna and D. R. Spearing. Nashville, TN, 2003.
- [6] J.S. McCloy, B.J. Riley, A. Goel, M. Liezers, M.J. Schweiger, C.P. Rodriguez, P. Hrma, D.-S. Kim, W.W. Lukens, A.A. Kruger, Environ. Sci. Technol. 46(22) (2012) 12616-12622.
- [7] B.J. Riley, J.S. McCloy, A. Goel, M. Liezers, M.J. Schweiger, J. Liu, C.P. Rodriguez, D.-S. Kim, J. Am. Ceram. Soc. 96(4) (2013) 1150-1157.

- [8] C.M. Jantzen, M.E. Smith, D.K. Peeler, pp. 141-152, Proc. of the Environmental Issues and Waste Management Technologies in the Ceramic and Nuclear Industries X, 168. Edited by J. D. Vienna, C. C. Herman, and S. Marra. Indianapolis, IN, 2004.
- [9] D. Caurant, P. Loiseau, O. Majerus, V. Aubin-Chevaldonnet, I. Bardez, A. Quintas, Glasses, Glass-Ceramics and Ceramics for Immobilization of Highly Radioactive Nuclear Wastes, pp. 248-250. New York: Nova Science Publishers (2009).
- [10] G. Calas, M. Le Grand, L. Galois, D. Ghaleb, J. Nucl. Mater. 322(1) (2003) 15-20.
- [11] G.N. Greaves, J. Non-Cryst. Solids 71(1-3) (1985) 203-217.
- [12] R.K. Mishra, K.V. Sudarsan, P. Sengupta, R.K. Vatsa, A.K. Tyagi, C.P. Kaushik, D. Das, K. Raj, J. Am. Ceram. Soc. 91(12) (2008) 3903-3907.
- [13] C.Z. Soderquist, M.J. Schweiger, D.-S. Kim, W.W. Lukens, J.S. McCloy, submitted to J. Nucl. Mater. (2013).
- [14] F.M. Mann. 2004. Annual Summary of the Integrated Disposal Facility Performance Assessment for 2004. DOE/ORP-2000-19, Rev. 4. CH2M Hill Hanford Group, Richland, WA.
- [15] P.R. Hrma. 2010. Retention of Halogens in Waste Glass. PNNL-19361. Pacific Northwest National Laboratory, Richland, WA.
- [16] S.N. Crichton, M.F. Savage, M. Tomozawa. 1995. In Proc. of the Environmental Issues and Waste Management Technologies in the Ceramic and Nuclear Industries: Ceramic Transactions, 61. pp. 291-298, Edited by V. Jain and R. Palmer. The American Ceramics Society, Inc., Westville, OH.
- [17] H. Abramowitz, M. Brandys, R. Cecil, N. D'Angelo, K.S. Matlack, I.S. Muller, I.L. Pegg, R.A. Callow, I. Joseph. 2012. Technetium Retention in WTP LAW Glass with Recycle

Flow-Sheet DM10 Melter Testing VSL-12R2640-1 Rev. 0. RPP-54130. Washington River Protection Solutions, Richland, WA.

- [18] S.N. Crichton, T.J. Barbieri, M. Tomozawa. 1995. In Proc. of the Environmental Issues and Waste Management Technologies in the Ceramic and Nuclear Industries: Ceramic Transactions, 61. pp. 283-290, Edited by V. Jain and R. Palmer. The American Ceramics Society, Inc., Westville, OH.
- [19] B.J. Riley, B.T. Rieck, J.S. McCloy, J.V. Crum, S.K. Sundaram, J.D. Vienna, J. Nucl. Mater. 424(1-3) (2012) 29-37.
- [20] W.M. Haynes, Y.-R. Luo (eds.), CRC Handbook of Chemistry and Physics, 91st ed. Boca Raton, FL: CRC Press/Taylor and Francis (2011).
- [21] P.L. Gassman, J.S. McCloy, C.Z. Soderquist, M.J. Schweiger, submitted to J. Raman Spectroscopy.
- [22] C.F. Brown, K.N. Geiszler, T.S. Vickerman, Anal. Chem. 77(21) (2005) 7062-7066.
- [23] S. Webb, http://ssrl.slac.stanford.edu/~swebb/spdocs/sixpack_documentation.htm, 2010.
- [24] B. Ravel, M. Newville, Phys. Scripta T115 (2005) 1007-1010.
- [25] Y.S. Shimamoto, Y. Takahashi, Anal. Sci. 24(3) (2008) 405-409.
- [26] W.A. Reed, I. May, F.R. Livens, J.M. Charnock, A.P. Jeapes, M. Gresley, R.M. Mitchell, P. Knight, J. Anal. At. Spectrom. 17(5) (2002) 541-543.
- [27] M. Fuhrmann, S.A. Bajt, M.A.A. Schoonen, Appl. Geochem. 13(2) (1998) 127-141.
- [28] D. Kim, M.J. Schweiger, J. Non-Cryst. Solids 379 (2013) 123-126.
- [29] R.W. Cheary, A.A. Coelho, J.P. Cline, J. Res. Natl. Inst. Stand. Technol. 109(1) (2004) 1-25.
- [30] M.T. Weller, G. Wong, Eur. J. Solid State Inorg. Chem. 26 (1989) 619-633.

DISCLAIMER

This document was prepared as an account of work sponsored by the United States Government. While this document is believed to contain correct information, neither the United States Government nor any agency thereof, nor the Regents of the University of California, nor any of their employees, makes any warranty, express or implied, or assumes any legal responsibility for the accuracy, completeness, or usefulness of any information, apparatus, product, or process disclosed, or represents that its use would not infringe privately owned rights. Reference herein to any specific commercial product, process, or service by its trade name, trademark, manufacturer, or otherwise, does not necessarily constitute or imply its endorsement, recommendation, or favoring by the United States Government or any agency thereof, or the Regents of the University of California. The views and opinions of authors expressed herein do not necessarily state or reflect those of the United States Government or any agency thereof or the Regents of the University of California.